Formylglycinamide ribonucleotide amidotransferase from *Salmonella typhimurium*: role of ATP complexation and the glutaminase domain in catalytic coupling

Ajay Singh Tanwar,[a] Marya Morar,[b] Santosh Panjikar[c] and Ruchi Anand[a]*

[a]Department of Chemistry, Indian Institute of Technology, IIT-Bombay, Mumbai 400 076, India, [b]Department of Chemistry and Chemical Biology, Cornell University, Ithaca, NY 14853, USA, and [c]Australian Synchrotron, 800 Blackburn Road, Clayton, VIC 3168, Australia

Correspondence e-mail: ruchi@chem.iitb.ac.in

Formylglycinamide ribonucleotide (FGAR) amidotransferase (FGAR-AT) takes part in purine biosynthesis and is a multidomain enzyme with multiple spatially separated active sites. FGAR-AT contains a glutaminase domain that is responsible for the generation of ammonia from glutamine. Ammonia is then transferred *via* a channel to a second active site located in the synthetase domain and utilized to convert FGAR to formylglycinamidine ribonucleotide (FGAM) in an adenosine triphosphate (ATP) dependent reaction. In some ammonia-channelling enzymes ligand binding triggers interdomain signalling between the two diverse active centres and also assists in formation of the ammonia channel. Previously, the structure of FGAR-AT from *Salmonella typhimurium* containing a glutamyl thioester intermediate covalently bound in the glutaminase active site was determined. In this work, the roles played by various ligands of FGAR-AT in inducing catalytic coupling are investigated. Structures of FGAR-AT from *S. typhimurium* were determined in two different states: the unliganded form and the binary complex with an ATP analogue in the presence of the glutamyl thioester intermediate. The structures were compared in order to decipher the roles of these two states in interdomain communication. Using a process of elimination, the results indicated that binding of FGAR is most likely to be the major mechanism by which catalytic coupling occurs. This is because conformational changes do not occur either upon formation of the glutamyl thioester intermediate or upon subsequent ATP complexation. A model of the FGAR-bound form of the enzyme suggested that the loop in the synthetase domain may be responsible for initiating catalytic coupling *via* its interaction with the N-terminal domain.

1. Introduction

Amidotransferases belong to a group of enzymes responsible for the catalysis of various amination reactions (Mouilleron & Golinelli-Pimpaneau, 2007). Amidotransferases can be divided into two major structurally diverse classes, both of which utilize the thiol group of a conserved cysteine residue to initiate a nucleophilic attack on the δ-carbonyl group of glutamine, resulting in the release of ammonia. Class I amidotransferases belong to the triad glutaminase family, which contain histidine, cysteine and glutamic acid residues responsible for catalyzing ammonia production. In contrast, class II enzymes contain an N-terminal cysteine residue that is activated for the same function (Massière & Badet-Denisot, 1998). Most amidotransferases work in consort with other enzymes and in several cases are part of a multidomain assembly generally consisting

of several active sites: one active site generates ammonia from glutamine and the ammonia is then channelled to another active site containing an acceptor molecule to be aminated. Based on the reported structures, the ammonia channel traverses anywhere from 10 to 40 Å and the catalytic activities of the two sites are thought to be coupled (Huang *et al.*, 2001; Mouilleron & Golinelli-Pimpaneau, 2007; Raushel *et al.*, 1999).

To prevent wasteful production of ammonia, most multi-domain proteins with coupled amidotransferase domains adopt an inactive conformation in the absence of their substrates (Huang *et al.*, 2001; Mouilleron & Golinelli-Pimpaneau, 2007). There are several mechanisms for activation of these enzymes and specific conformational changes associated with ligand binding are responsible for interdomain signalling. However, these changes are not conserved among the various amido-transferases and vary depending upon the architecture of the acceptor domain (Raushel *et al.*, 2003). Any of the ligands involved in the reaction parent to the multidomain system can be responsible for triggering the conformation change necessary for communication between the domains. In some of these systems binding of glutamine results in reorganization of the glutaminase active-site residues (Myers *et al.*, 2003, 2005; Willemoës *et al.*, 2005). Glutamine binding can subsequently be communicated to the acceptor domain *via* conformational changes (Goto *et al.*, 2004). However, in some cases it is the binding of substrate to the acceptor domain that is crucial in initiating interdomain communication between the two diverse active centres (Holden *et al.*, 1999; Mouilleron & Golinelli-Pimpaneau, 2007). The mechanism of catalytic

coupling among this diverse set of acceptor domains coupled with a subset of glutaminase domains can thus follow a wide range of rearrangements and differs from system to system. Since most of the conformational changes involved in catalytic coupling are transient and occur during the time scale of the reaction, it is often challenging to map the state that induces communication between two spatially separated active sites.

Formylglycinamide ribonucleotide (FGAR) amidotrans-ferase (FGAR-AT) catalyzes the ATP-dependent amidation of FGAR to formyl glycinamidine ribonucleotide (FGAM) (Fig. 1a; Levenberg *et al.*, 1957). This reaction is the fourth step in the *de novo* purine-biosynthetic pathway, which is a ten-step synthesis of inosine monophosphate from phosphoribosyl pyrophosphate (Zhang *et al.*, 2008). Two types of FGAR-AT, also known as PurL, have been characterized. In Gram-negative bacteria and eukaryotes FGAR-AT consists of a single polypeptide chain encoded by single gene, *purL*, and is referred to as large PurL (lgPurL). The structure of lgPurL from *Salmonella typhimurium* (StPurL) has previously been described (Anand, Hoskins, Stubbe *et al.*, 2004). StPurL contains three major domains: the N-terminal domain, the FGAM synthetase domain and the C-terminal glutaminase domain. The active sites of the FGAM synthetase and the glutaminase domains have been proposed to be connected *via* an ammonia channel and are catalytically coupled. The N-terminal domain is thought to play a role in the formation of the ammonia channel and communication between the two active sites (Anand, Hoskins, Stubbe *et al.*, 2004).

In Gram-positive bacteria and archaea, three separate gene products encoded by the genes *purL*, *purQ* and *purS* come
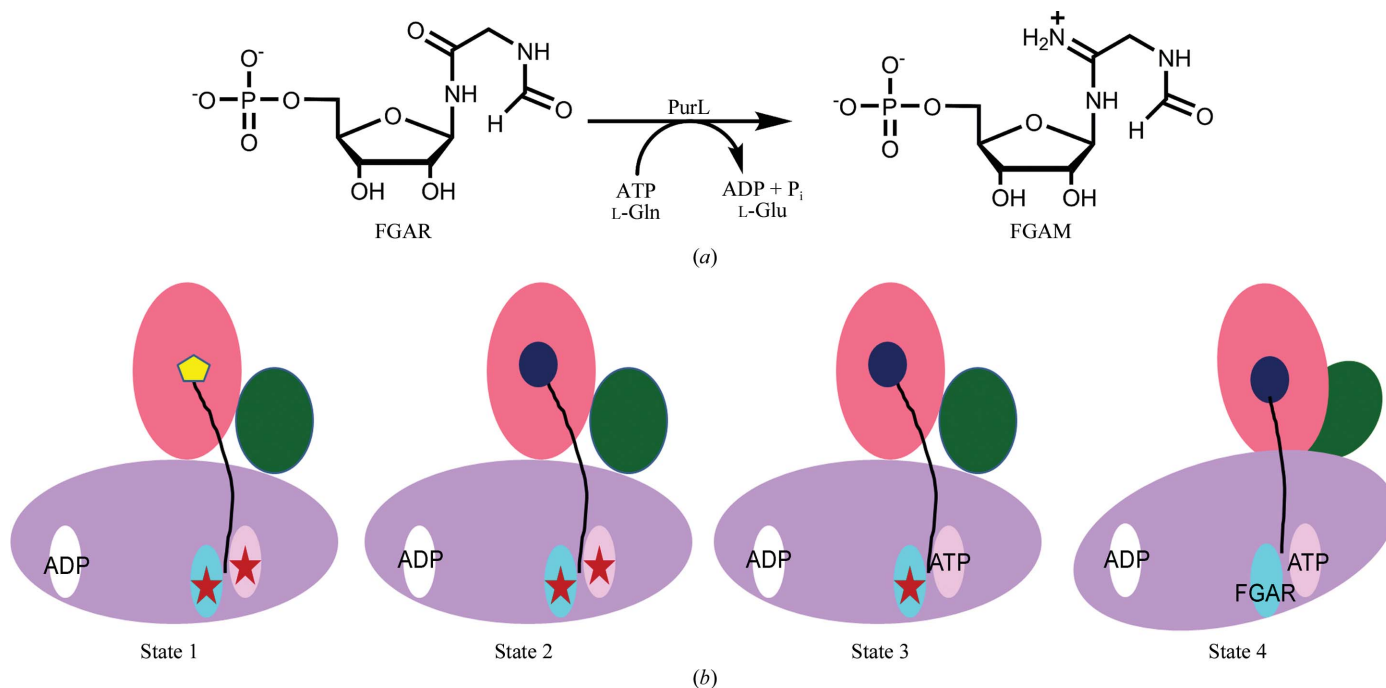
Figure 1
(*a*) Reaction catalyzed by PurL. (*b*) Model of the proposed states involved in catalytic coupling in PurL; the glutaminase domain is shown in pink, the N-terminal domain in green, the FGAM synthetase domain in light purple, the auxiliary ADP-binding site in white, the FGAR-binding site in cyan and the ATP-binding site in light pink. A black line represents the path followed by ammonia. The presence of the glutamyl thioester intermediate is shown as a blue sphere. The yellow pentagon indicates an empty amidotransferase site.

Table 1
Data-collection and refinement statistics.

Values in parentheses are for the highest resolution bin.

	Unliganded StPurL (PDB entry 3ugj)	StPurL–glycerol (PDB entry 3ujn)	StPurL–AMPPNP (PDB entry 3umm)
Data collection			
Resolution (Å)	1.80	2.98	3.35
Total No. of reflections	601882	200726	234506
No. of unique reflections	162818	69080	29368
Completeness (%)	99.2 (98.7)	98.1 (98.1)	99.6 (100)
Multiplicity	3.7 (3.8)	2.9 (2.8)	8.0 (8.0)
R_{merge}† (%)	8.1 (38.7)	13.3 (44.3)	15.5 (35.5)
Refinement statistics			
Total No. of non-H atoms	10759	10205	10131
No. of protein atoms	9884	9910	9909
No. of ligand atoms	55	40	71
No. of water atoms	820	255	152
No. of reflections in refinement	157090	34973	25157
No. of reflections in test set	15661	3470	2489
R_{factor}‡ (%)	21.1	20.8	19.6
R_{free}§ (%)	24.0	26.4	27.3
R.m.s.d. from ideal geometry			
Bonds (Å)	0.006	0.011	0.011
Angles (°)	1.37	1.40	1.40
Average B factor (Å^2)	16.4	27.8	30.4
Ramachandran plot			
Most favoured region (%)	94.8	93.8	93.2
Additional allowed region (%)	4.6	5.2	5.3
Disallowed region (%)	0.6	1.0	1.5

† $R_{merge} = \sum_{hkl} \sum_i |I_i(hkl) - \langle I(hkl)\rangle| / \sum_{hkl} \sum_i I_i(hkl)$, where $\langle I(hkl)\rangle$ is the mean intensity of the i reflections with intensity $I_i(hkl)$ and common indices hkl. ‡ R factor = $\sum_{hkl} ||F_{obs}| - |F_{calc}|| / \sum_{hkl} |F_{obs}| \sum_{hkl}$, where F_{obs} and F_{calc} are observed and calculated structure factors, respectively. § For R_{free} the sum extends over a subset of reflections (10%) that were excluded from all stages of refinement.

together to form a complex in a metabolite-dependent fashion and encode proteins referred to here as small PurL (smPurL), PurQ and PurS, respectively (Hoskins *et al.*, 2004). smPurL is responsible for FGAM synthetase activity and five ligand-complexed structures of smPurL from *Thermotoga maritima* (TmPurL) have provided a detailed description of this enzyme (Morar *et al.*, 2006). PurS, the structure of which is also known, is homologous to the N-terminal domain of lgPurL and hence is thought to play a similar role (Anand, Hoskins, Bennett *et al.*, 2004).

Previously determined structures of ATP and FGAR complexes together with kinetic studies have shed light on the substrate-binding modes and point towards a partially compulsory ordered mechanism (Li & Buchanan, 1971; Morar *et al.*, 2006). However, very little information is available regarding the orchestration of the events that lead to formation of the ammonia channel and the mechanism of catalytic coupling. In an effort to unravel the sequence of conformational changes upon binding of an individual ligand, we propose four plausible states of ligand occupancy (Fig. 1*b*). The structure of StPurL was solved in the presence of glutamine and adenosine 5′-(*β,γ*-imido)triphosphate (AMPPNP), a nonhydrolysable form of ATP, in order to understand the structural changes upon ATP binding. Furthermore, the structure of StPurL was solved in the apo form and compared with the previously determined structure of the glutamyl thioester-bound form of the enzyme (Anand, Hoskins, Stubbe *et al.*, 2004; Schendel & Stubbe, 1986). A structure of the synthetase domain of TmPurL in complex with ATP and

FGAR is already available (Morar *et al.*, 2006). However, the structure of the liganded form of TmPurL is insufficient to provide information about interdomain communication upon ligand binding as it only consists of the FGAM synthetase domain. In this work, we present the structure of ATP in complex with lgPurL in the presence of all three domains and discuss the role played by ATP binding in catalytic coupling.

In the previously determined structures of both the TmPurLQS multiprotein complex (Morar *et al.*, 2008) and the single-chain multidomain protein StPurL (Anand, Hoskins, Stubbe *et al.*, 2004) the glutamyl thioester was found at the active site of the glutaminase domain; however, it was unclear whether this intermediate was important for complex formation in PurLQS or whether it plays an important role in catalytic coupling between the two active sites. Thus, the determination of an additional structure of the enzyme in the apo form in which both the catalytic sites are unoccupied would help to answer the above question.

2. Experimental procedures

2.1. Cloning, expression and purification of unliganded StPurL

The procedures for the cloning, expression and purification of StPurL have been reported previously (Anand, Hoskins, Stubbe *et al.*, 2004). The important difference between the reported protocol and the work described here is the dialysis step after protein purification. Purified StPurL was dialyzed

against 5 mM MgCl$_2$, 20 mM HEPES pH 7.2; glutamine was absent from the dialysis buffer.

2.2. Crystallization, data collection and processing, structure determination and refinement of unliganded StPurL and the AMPPNP-complexed form of StPurL

Three crystal structures are reported: the unliganded form of StPurL, the low-salt soaked form of StPurL and the low-salt StPurL–AMPPNP complex. The unliganded form of StPurL was crystallized following the published procedure using the hanging-drop vapour-diffusion method (Anand, Hoskins, Stubbe et al., 2004). Crystals grew within a week in the hexagonal space group $P6_5$, with unit-cell parameters a = 146.0, c = 141.2 Å, and were cryoprotected using well solution with the addition of 20% glycerol. Data were obtained to a resolution of 1.8 Å using an R-AXIS IV detector, 1° oscillation, 15 min exposure time and a crystal-to-detector distance of 120 mm. The data were indexed, integrated and scaled using *HKL*-2000 (Otwinowski & Minor, 1997).

Crystals of a sulfate-free complex were prepared by dilution with low-salt solvent. Crystals of StPurL grown under high-sulfate conditions were soaked in a cryoprotectant solution containing only 20% glycerol prepared in buffer at pH 7.5 for a period of 5 min. Data were collected on beamline BM-14 at the European Synchroton Radiation Facility, Grenoble using a 225 mm MAR CCD detector, 0.5° oscillation, an exposure time of 10 s and a crystal-to-detector distance of 210 mm and were processed as described below. The data were collected at a wavelength of 0.82 Å and the crystals diffracted to a resolution of 2.98 Å.

For the StPurL–AMPPNP complex, the crystals were grown as described above and were subsequently soaked in a solution consisting of 20% glycerol and 25 mM HEPES pH 7.0 for 5 min followed by soaking in 20% glycerol containing 5 mM AMPPNP. A data set for the StPurL–AMPPNP complex extending to a resolution of 3.35 Å was collected on beamline BM-14 at the European Synchroton Radiation Facility, Grenoble using a 225 mm MAR CCD detector, 0.5° oscillation, an exposure time of 10 s and a crystal-to-detector distance of 210 mm. The resolution of the complex is lower than that of the native crystal because the process of double soaking under low-salt conditions resulted in slight degradation of the crystals and thus decreased diffraction quality. The StPurL–AMPPNP crystals also belonged to the hexagonal space group $P6_5$, with unit-cell parameters a = 148.6, c = 142.0 Å. The data were indexed, integrated and scaled using *MOSFLM* (Leslie, 1997) and the *CCP*4 suite of programs was used for further manipulation of the data (Winn et al., 2011). Data-collection statistics are summarized in Table 1.

The *Auto-Rickshaw* automated crystal structure-determination software (Panjikar et al., 2005) was used to confirm at the beamline that the AMPPNP complex had been captured.
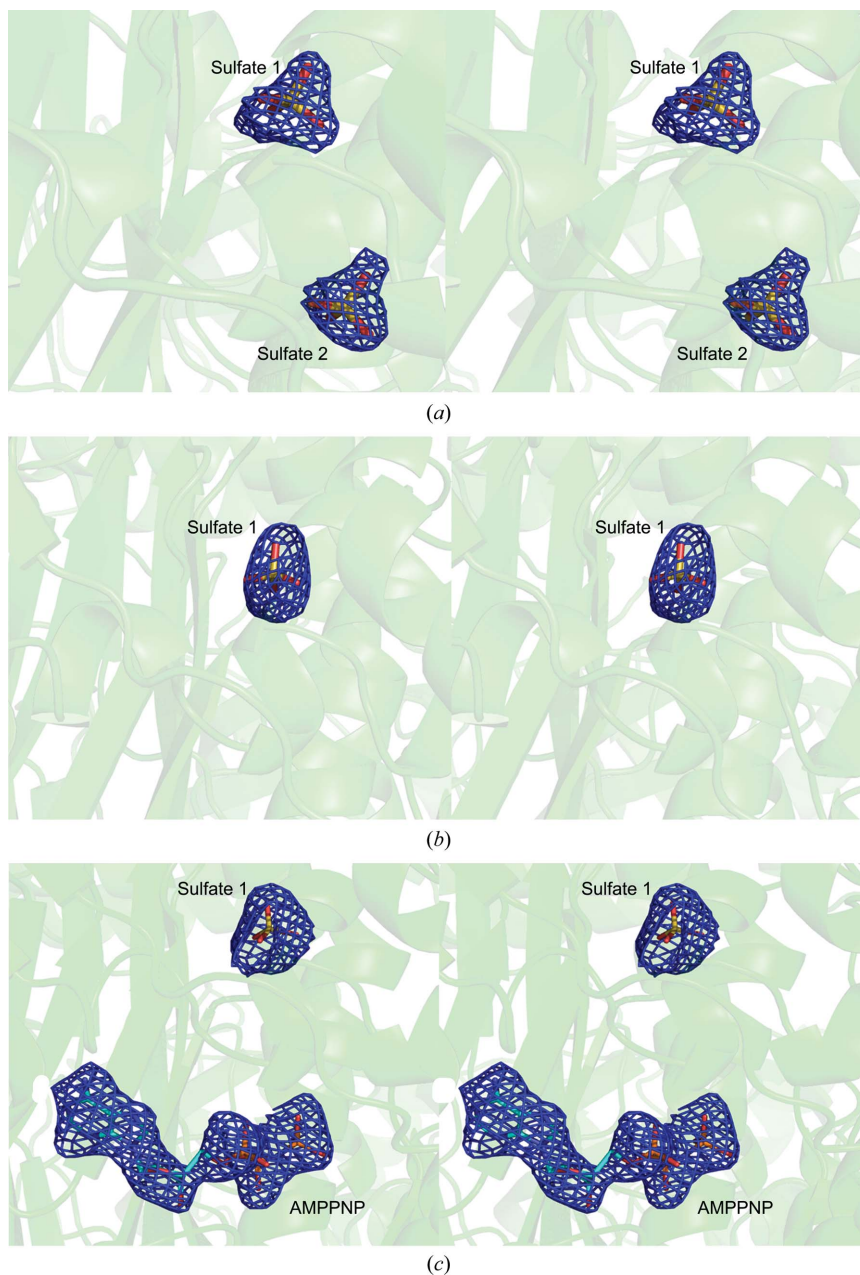
Figure 2
Strategy for determination of the AMPPNP complex. (a) The $F_o − F_c$ density at 3σ for StPurL crystals grown under high-salt conditions is shown. Two sulfate ions are bound in the active-site region: sulfate 1 and sulfate 2. (b) Crystals soaked under low-salt conditions have only one sulfate ion bound (sulfate 1). (c) The $F_o − F_c$ density at 2.8σ shows density for AMPPNP and sulfate ion 1. In all panels the S atom is shown in yellow, O atoms are shown in red, C atoms are shown in light blue and N atoms are shown in blue.

The structures of unliganded StPurL and the StPurL–AMPPNP complex were determined by performing rigid-body refinement of the published structure of StPurL (PDB entry 1t3t; Anand, Hoskin, Stubbe *et al.*, 2004) against the data collected. The *CNS* program suite was used for refinement (Brünger *et al.*, 1998). The initial model was subsequently refined by performing rounds of annealing, *B*-factor refinement and minimization and was followed by manual model building using the programs *O* (Jones *et al.*, 1991) and *Coot* (Emsley *et al.*, 2010). Water molecules were added during the later rounds of refinement. The final refinement statistics are listed in Table 1. The validity of the model was verified using *PROCHECK* (Laskowski *et al.*, 1993).

2.3. Molecular modelling of the StPurL synthetase loop

The synthetase loop of StPurL (residues 448–475) was modelled using the homology-modelling program *MODELLER* 9v5 (Fiser *et al.*, 2000). The template for loop modelling was obtained from the published structure of TmPurL (PDB entry 2hs4; Morar *et al.*, 2006). Firstly, the loop sequence to be modelled was aligned (target: UniProt ID P74881) with the corresponding loop-region residues 183–203 in TmPurL (template: UniProt ID Q9X0X3). The sequence was taken in FASTA format. In the second step a framework (hydrogen bonds, bond lengths, dihedral angles) was built for the target based on the template. In the final step spatial restraints of the structure were obtained. After a convergence test, the best model with reasonable geometry was selected for further analysis.

2.4. Figure preparation

The figures were prepared using the program *PyMOL* (DeLano, 2002).

3. Results and discussion

3.1. Quality assessment of the unliganded StPurL and AMPPNP structures

In this work, we present three structures of StPurL: in the unliganded form with no ligands bound to the respective active sites, in the low-salt form with the spurious sulfates partially removed and in the low-salt binary complex with the thioester intermediate in the glutaminase active site and the AMPPNP complex bound to the FGAM synthetase site. All residues except for 448–466 and 449–466 were included in the final models of unliganded StPurL and the StPurL–AMPPNP complex, respectively. The missing residues are located in a disordered loop that becomes visible upon FGAR binding, as observed in the previously determined structure of TmPurL complexed with FGAR (Morar *et al.*, 2006). Cys1135 in un-liganded StPurL, which is located in the active site of the glutaminase domain, has disallowed geometry, as previously observed for the glutamyl thioester intermediate; however, the electron density for this residue is clear (Anand, Hoskins, Stubbe *et al.*, 2004). There are also some solvent-exposed residues, which show disallowed geometry mostly because of

poor ordering. Owing to the lower resolution of the StPurL–AMPPNP complex structure the number of poorly modelled residues is slightly increased, thus resulting in a slight increase in the total number of disallowed residues, as reflected in Table 1. The final *R* factor for the unliganded StPurL structure is 21.1% and R_{free} is 24.0%, whereas the final *R* factor for the StPurL–AMPPNP complex is 19.6% and R_{free} is 27.3%.

3.2. Strategy for structure determination of the AMPPNP complex

Screening of various conditions always yielded crystals of StPurL under high ammonium sulfate or lithium sulfate conditions. The current crystallization conditions consisted of 2 *M* ammonium sulfate solution. In the absence of any complexes of lgPurL, these sulfate ions (labelled sulfate 1 and sulfate 2 in Fig. 2*a*) were helpful in revealing the positions of the two phosphate ions and of the substrate FGAR and the γ-phosphate of ATP, respectively (Anand, Hoskins, Stubbe *et al.*, 2004). The high salt concentration in the crystallization conditions impeded the successful incorporation of substrate. Therefore, soaking with AMPPNP under low-salt conditions was tried. The electron density indicated that sulfate 2 was displaced from its original position by solvent; however, sulfate 1 remained bound (Fig. 2*b*). Analysis of the structure revealed that sulfate 1 is more tightly coordinated *via* hydrogen-bonding interactions with the surrounding residues compared with sulfate 2. Sulfate 2 is also closer to the surface and thus is readily exchanged. The same strategy was subsequently followed to obtain the StPurL–AMPPNP complex. As shown in Fig. 2(*c*), the ATP analogue binds in the available position, with the γ-phosphate of ATP occupying the position vacated by sulfate 2. Longer soaking in low-salt glycerol solution resulted in further degradation of diffraction quality. In addition, any efforts to subsequently soak crystals with FGAR resulted in instantaneous decomposition of the crystals, indicating that FGAR binding may cause a major conformational change.

3.3. Comparison of the thioester-intermediate structure (state 2) with those of unliganded StPurL (state 1) and the binary AMPPNP complex (state 3)

A comparison of the structures of unliganded StPurL and of the binary complex of the thioester intermediate with AMPPNP with that of the previously determined structure in the presence of the glutamyl thioester intermediate (Anand, Hoskins, Stubbe *et al.*, 2004) was performed. The root-mean-square deviations (r.m.s.d.s) between the structures were 0.2 and 0.45 Å over 1277 C^α atoms, respectively. In order to look for concerted and possibly subtle changes in the structures that would be indicative of domains moving with respect to one another, the r.m.s.d.s between the structures were plotted as depicted in Fig. 3(*a*). The plots revealed that compared with the unliganded form the r.m.s.d.s are slightly higher for the binary complex. The detected differences in both structures are the consequence of some flexibility in solvent-exposed loop regions rather than orchestrated domain motions. The
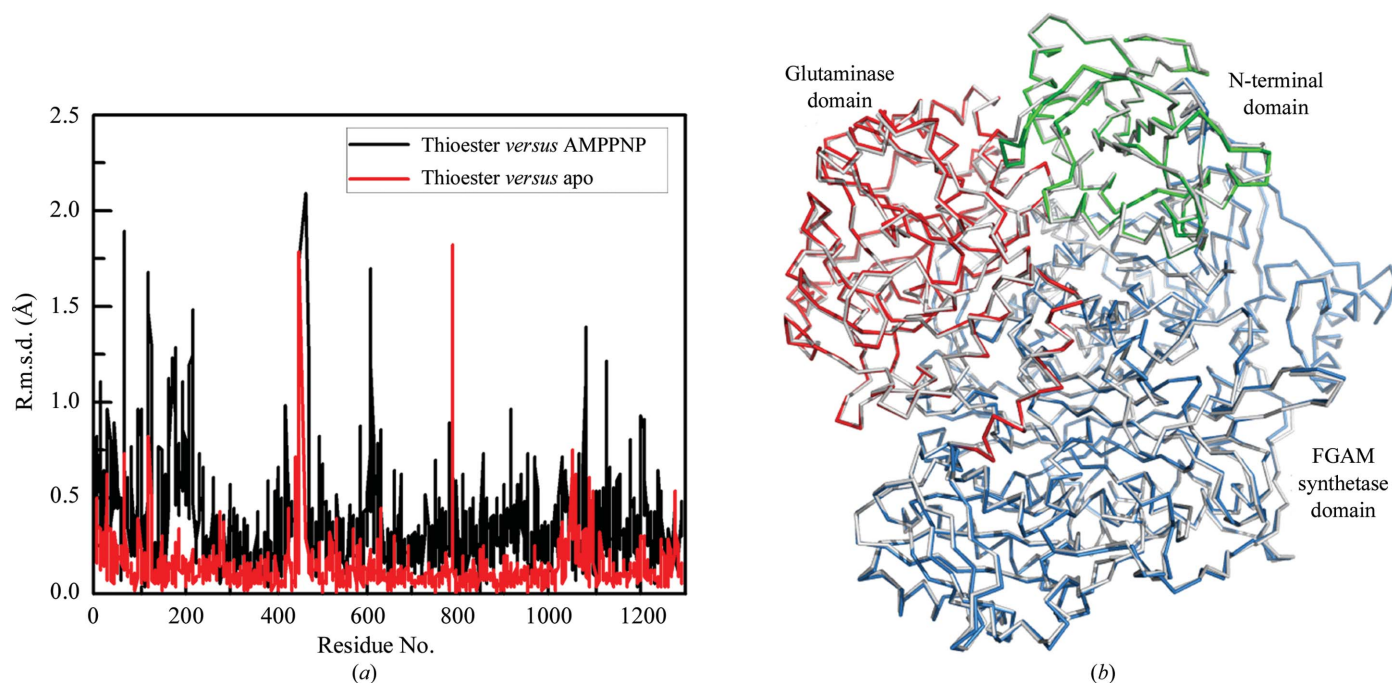
Figure 3
Comparison between different states. (a) The graph depicts the r.m.s.d. of Cα atoms between different states of ligand occupation. The r.m.s.d. between the glutamyl thioester form (PDB entry 1t3t) and the apo form (PDB entry 3ugj) is shown in red, while that between the glutamyl thioester form and the StPurL–AMPPNP binary complex (PDB entry 3umm) is shown in black. (b) The ribbon representation shows the superposition of the glutanyl thioester form and the StPurL–AMPPNP binary complex form. Each domain of thioester form is represented in a different colour (the N-terminal domain in green, the FGAM synthetase domain in sky blue and the glutaminase domain in red). The binary complex is shown in grey.

region that shows high r.m.s.d.s in both structures is near the highly flexible FGAR-binding loop region in the synthetase domain (Morar *et al.*, 2006). The results suggest that formation of the glutamyl thioester intermediate does not trigger any domain movement when compared with the unliganded protein. Therefore, the binding of glutamine alone in the glutaminase active site is unlikely to activate catalytic coupling between the FGAM synthetase and glutaminase domains. The trapping of the glutamyl thioester intermediate upon addition of glutamine further indicates that the enzyme is in an unproductive conformation, as it is unable to fully hydrolyse glutamine. In the AMPPNP complex structure there is an overall slight movement of the structure, with most of the changes concentrated in the N-terminal region and a few at the extreme C-terminal end of the protein, which is in close proximity to the N-terminal region. This movement corresponds to a slight overall repositioning of the N-terminal domain of PurL, which leads to a minor opening of the N-terminal domain. Although there is no major shift in the N-terminal domain, it is very likely that the slight alteration in this region upon ATP binding is indicative of a subsequent major movement that is orchestrated upon FGAR binding. Thus, both trapped forms of the enzyme essentially present the enzyme in a similar conformation and the comparison seems to provide pointers to regions that are likely to undergo major movement upon FGAR binding.

Additionally, the FGAM synthetase active site in the unliganded structure is filled with water molecules. The active site of the glutaminase domain is similar to that of the

reported StPurL structure (Anand, Hoskins, Stubbe *et al.*, 2004; Fig. 4). Dialysis against glutamine-free buffer was successful in removing most of the bound glutamyl thioester intermediate at Cys1135. While there is a peak in the $F_o - F_c$ density with a peak height of close to 2.5σ, indicating that the site is not completely empty, a comparison of this density with that when the active site is fully occupied reveals that the amount of the intermediate present is negligible. A water molecule positioned to perform hydrolysis of the glutamyl thioester intermediate in the complexed structure is conserved in the unliganded structure (Anand, Hoskins, Stubbe *et al.*, 2004). If the role of this water is indeed to hydrolyze the glutamyl thioester intermediate, the unliganded structure indicates that the water is positioned prior to the binding of glutamine.

3.4. Structure of the active site of the StPurL–AMPPNP complex

The FGAM synthetase domain of StPurL consists of four subdomains, the A1 and B1 subdomains and the A2 and B2 subdomains, and exhibits gene duplication, with the two halves related by pseudo-twofold symmetry. The β-sheet region of the A1 and A2 subdomains comes together to form a central hydrophobic barrel that is flanked by helices on either side (Anand, Hoskins, Stubbe *et al.*, 2004). The FGAM synthetase-domain active site is sandwiched between the cleft formed by the A2, A1 and B1 subdomains, while the other gene-duplicated half binds an auxiliary ADP, the function of which

remains elusive (Anand, Hoskins, Stubbe *et al.*, 2004). In order to study the conformational changes associated with ATP binding, the structure of StPurL was solved as a complex with AMPPNP. Fig. 2(c) shows the $F_o - F_c$ map at 2.8σ for the AMPPNP complex. A comparison of the previously reported structure of the unliganded form of StPurL with that of the StPurL–AMPPNP complex shows that almost no local conformational changes occur upon ATP binding. The ATP moiety fits into the active site of the FGAM synthetase domain that is encompassed by helices $\alpha9$ and $\alpha11$. The adenine base is packed against β-strands 27 and 28 belonging to the A2 subdomain and helix $\alpha9$ of the A1 subdomain, as shown in Fig. 5(a). The adenine ring is surrounded by a hydrophobic pocket formed by residues Phe222, Phe238, Tyr256 and Ile772. The ribose ring of the AMPPNP ligand is closer to residues Asn259, Asp258 and Tyr256, which lie on a loop spanning residues 247–261. The 3′-hydroxyl group of the ribose ring is anchored *via* hydrogen-bonding interactions with the carbonyl O atom of residue Asp258 (Fig. 5b). The phosphate tail of AMPPNP in the StPurL–AMPPNP complex exhibits hydrogen-bonding interactions with residues of the strand $\beta11$–loop–helix $\alpha11$ region. One of the O atoms of the γ-phosphate group of the AMPPNP tail forms a hydrogen bond to the carboxylic group of the side chain of Glu294, while the other O atom forms hydrogen-bonding interactions to Asp502 and Asp318. The negatively charged phosphate region is stabilized *via* interaction with a magnesium ion which is missing in the current structure. The conserved negatively charged residues in this region hydrogen-bond to the magnesium ion and strengthen ATP binding. Asp318 lies on helix $\alpha11$, is conserved among all PurLs and is part of the signature sequence DX_4GAXP found in PurL/PurM superfamily members (Kappock *et al.*, 2000; Li *et al.*, 1999; McCulloch *et al.*, 2008; Reissmann *et al.*, 2003). The O atoms of the β-phosphate group of the phosphate tail are stabilized by interactions with positively charged N atoms of residues Lys292 and Lys776. The O atoms of the α-phosphate group of the phosphate tail interact with the N atom of residue His219. Figs. 5(a) and 5(b) show the detailed interactions of the AMPPNP complex with the surrounding StPurL residues.

Figure 4
Active site of the StPurL glutaminase domain. (a) Superposition of the active site of StPurL bound to the glutamyl thioester intermediate (grey and green) with unliganded StPurL (blue). The electron density is insufficient for modelling the glutamyl thioester intermediate. (b) Active site of StPurL. The difference electron density illustrates that the glutamyl thioester intermediate is present.
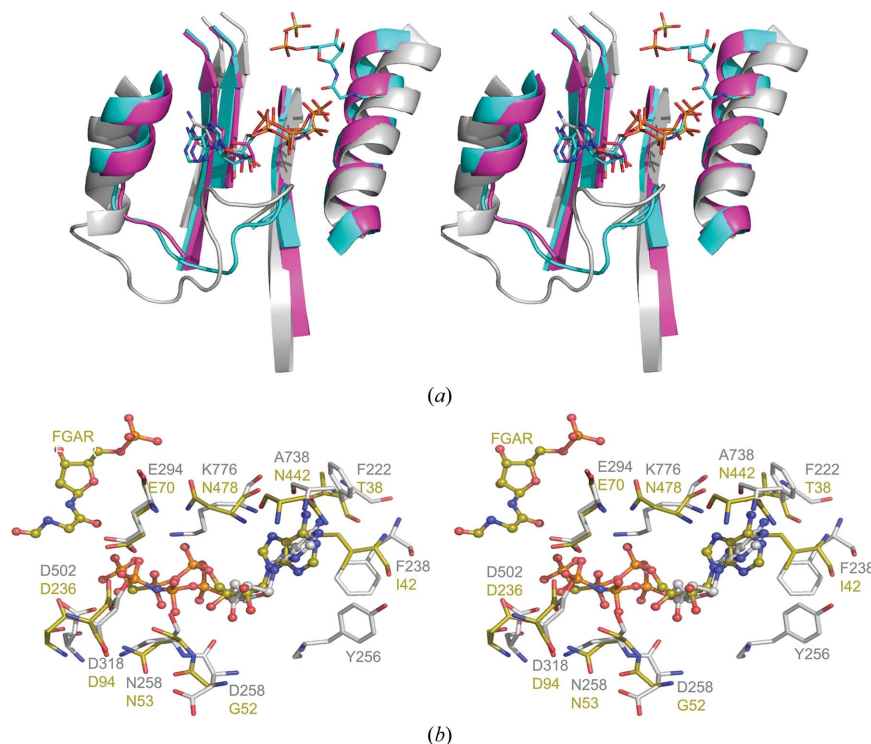
Figure 5
View of the ATP-binding site. (a) Superposition showing a comparison between the StPurL–AMPPNP complex (grey), the H72A TmPurL–AMPPCP complex (magenta) and the TmPurL–FGAR–AMPPCP complex (cyan). The loop is disordered in the H72A TmPurL–AMPPCP complex. (b) Comparison of ATP-binding sites, with the C atoms of the StPurL–AMPPNP complex in grey and those of the TmPurL–FGAR–AMPPCP ternary complex in yellow. In all figures the N atoms are shown as blue sticks and the O atoms are shown in red.

3.5. Comparison of the StPurL–AMPPNP structure with those of the TmPurL–AMPPCP and TmPurL–AMPPCP–FGAR complexes

Superposition (Figs. 5a and 5b) of the StPurL–AMPPNP complex with the complexes of TmPurL (TmPurL–AMPPCP,

Tanwar *et al.* · Formylglycinamide ribonucleotide amidotransferase

H72A TmPurL–ATP and TmPurL–FGAR–AMPPCP) indicates that the StPurL–AMPPNP complex is almost identical to the TmPurL–FGAR–AMPPCP ternary complex (Morar *et al.*, 2006). Although the sequence identity in this region between the two species is only 21.3%, the overall fold of the structures is similar. A superposition performed for the C$^\alpha$ atoms of residues 215–970 of StPurL with those of residues 2–603 of TmPurL shows that they superimpose with an r.m.s.d. of 2.3 Å. Fig. 5(*a*) shows that the secondary-structural elements in the ATP-binding regions of both species are broadly conserved. The flanking helix at the phosphate tail end of ATP, α11 in the case of StPurL, corresponding to α5 in TmPurL, is longer in StPurL. In StPurL the sequence DX_4GAXP is much more extended, with additional glycine residues inserted into this region, and corresponds to the sequence DX_6GAXP. Overall, the phosphate-binding region is mostly conserved in both species, with similar pattern of negatively and positively charged residues stabilizing the metal–phosphate complex.

The major differences in the ATP-binding region between these two complexes are in the adenine-binding pocket, together with some interactions in the ribose-binding region. The base of the ATP moiety in this class of proteins is in close proximity to a loop region present in both species. In the StPurL–AMPPNP complex this loop is 15 residues long and spans residues 247–261, but in the TmPurL ternary complex it is much shorter and consists of nine amino acids spanning residues 46–54. This loop region is always ordered in the case of lgPurL; however, this loop region remains completely disordered in the binary TmPurL–AMPCP complex and only becomes ordered upon FGAR binding, as seen in the TmPurL–AMPPCP–FGAR ternary complex (Fig. 5a). Owing to the longer length of this loop region in StPurL, this loop is oriented such that it is closer to the AMPPNP ligand in the StPurL complex compared with the corresponding TmPurL ternary complex. This reveals that the ligand pocket is narrower in the StPurL–AMPPNP complex and binds ATP more tightly than the TmPurL ternary complex. In the case of StPurL this loop region is important for stabilizing the ATP moiety and makes several interactions with the ATP molecule. However, in TmPurL this loop does not make any interactions with the ATP molecule even when it becomes ordered. The ribose ring of the StPurL–AMPPNP complex is closer to residues Asn259, Asp258 and Tyr256, which lie on this loop. The 3′-hydroxyl group of the ribose ring is anchored *via* hydrogen-bonding interactions of the carbonyl O atom of residue Asp258. This is very similar to what has been observed in other ATP-binding proteins in which acidic residues stabilize the hydroxyl group of the ribose moiety (Schulz, 1992). In addition, this loop region is also closer to the adenine ring in the StPurL–AMPPNP complex. Tyr256, which lies on this loop, forms part of the hydrophobic pocket of adenine and makes hydrophobic stacking interactions with the adenine ring. No counterpart residue exists in TmPurL, and thus StPurL has additional stabilizing interactions in this region. A comparison of the two active sites shown in Fig. 5(*b*) also indicates that the adenine-binding hydrophobic pocket in the two proteins is not conserved. In the StPurL–AMPPNP

complex the adenine ring occupies a deeper hydrophobic pocket that stacks against the pyrimidine ring. However, in the case of the TmPurL complex the pocket is not as richly lined with hydrophobic residues. The overall comparison and analysis of the two structures reveal that no major conformational change is associated with ATP binding; therefore, FGAR is the most likely candidate for triggering catalytic coupling.

3.6. Implications of the unliganded and AMPPNP-complexed StPurL structures for catalytic coupling

In some amidotransferases the glutaminase domain becomes activated upon binding of the acceptor molecule in the distal active site responsible for the amination reaction (Mouilleron & Golinelli-Pimpaneau, 2007). For FGAR-AT, structural conformations are thought to occur in the domains of the enzyme that trigger catalytic coupling and ammonia-channel formation (Anand, Hoskins, Stubbe *et al.*, 2004; Hoskins *et al.*, 2004). As glutamine is required for complex formation in the PurLQS complex, it was thought that binding of this substrate in the glutaminase site may also promote such conformational rearrangement (Anand, Hoskins, Stubbe *et al.*, 2004). However, no conformational changes were observed between the structures of glutamyl thioester-bound and unbound forms of StPurL. It is evident that some interdomain communication exists between the two catalytic sites as in the absence of ATP and FGAR because the glutaminase domains of PurLs are unable to catalyze glutamine to glutamate and no ammonia production is observed. It is unlikely that the lack of observable conformation changes upon glutamine binding is a crystallization artefact because the intermediate-free protein was generated in solution and not in the crystal. The unliganded protein must therefore assume the same conformation that favours crystal growth when the intermediate is bound. It is more likely that the binding of substrates in the FGAM synthetase domain affects the conformation of the glutaminase domain and thereby activates catalysis. Such a mechanism would agree with previous observations of glutaminases being activated by the synthetase but not the converse (Mouilleron & Golinelli-Pimpaneau, 2007; Raushel *et al.*, 1999, 2003).

Further work performed on the StPurL–AMPPNP complex also did not result in any major conformational changes; thus, it is now clear that neither glutamine nor ATP plays a pivotal role in catalytic coupling. The addition of FGAR to crystals of StPurL always resulted in immediate decomposition of the crystals. This was one of the major reasons that the FGAR–AMPPNP ternary complex could not be captured in the StPurL system. Even crystals of catalytically dead forms of the enzyme in which the catalytic histidine residues His216 and His296 have been replaced by alanine residues are also destabilized in the presence of FGAR. This seems to strongly suggest that the role of FGAR binding involves more than just production of FGAM and that it is also key to the induction of catalytic coupling. In the case of TmPurL, an FGAR–AMPPCP ternary complex could be captured because the
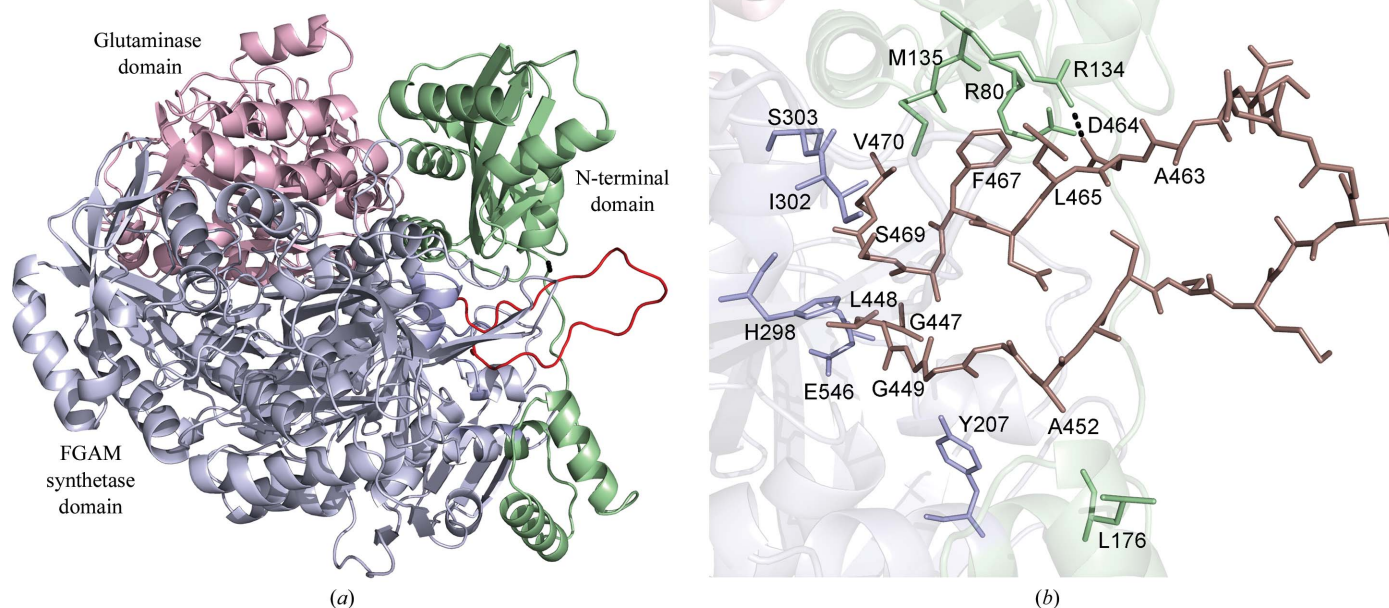
Figure 6
Proposed model. (*a*) StPurL with the modelled loop in red, the glutaminase domain in light pink, the FGAM synthetase domain in light blue and the N-terminal domain with extended loop and linker helices in light green. (*b*) Interaction of the modelled loop (dark salmon) with residues of the N-terminal domain and the FGAM synthetase domain. Interacting residues are shown in stick representation. Sticks are represented in the same domain colours as in (*a*).

three proteins PurS, PurQ and smPurL are the products of three separate genes and are likely to be catalytically inactive when present in isolation. Thus, capturing the TmPurL complex in the absence of PurS and PurQ mimics a state of StPurL in which catalytic coupling has been disabled. For a more complete characterization of the mechanism of catalytic coupling, a crystal structure of a complex of StPurL with FGAR and FGAR–ATP (state 4) is necessary since this would reveal the domain conformations that are necessary for catalytic coupling and activity. To obtain this structure, an inactive complex of the protein needs to be formed and further co-crystallization experiments need to be performed to explore new protein conformations and crystal forms that can accommodate the changes in the structure that occur upon catalytic coupling.

3.7. Proposed model for catalytic coupling

In the absence of the availability of the FGAR-bound form of StPurL, we modelled the missing loop-region residues 448–466 present in the FGAM synthetase domain of StPurL by using the loop-modelling feature in the homology-modelling software *MODELLER* (Fiser *et al.*, 2000). The conformation of the loop residues was obtained by comparison of this region with that of TmPurL; a structure of the synthetase domain of TmPurL complexed with ATP–FGAR is available (Morar *et al.*, 2006). The resulting model cannot provide direct information about the actual domain movements associated with FGAR binding, but it can provide clues about the additional interactions that are initiated upon ordering of this catalytic loop, which can then induce further interdomain communication with the other domains. The modelled loop is shown

in red in Fig. 6(*a*). The loop adopts an extended conformation away from the synthetase domain and seems to be mostly solvent-exposed. Ordering of residues 448–466 in the synthetase domain not only seems to be responsible for shielding of the substrate FGAR from the solvent, but also helps in communication of the acceptor binding. The loop adopts a conformation that is in close proximity to both the N-terminal domain (shown in light green in Fig. 6a) and the linker domain. Both these domains are hypothesized to play a pivotal role in catalytic coupling and in the formation of the ammonia channel. The model indicates that the guanidinium group of Arg134 in the N-terminal domain makes a hydrogen-bonding interaction with the acidic carboxyl group of loop residue Asp464. In addition, Phe467 and Leu465 in the loop region also form hydrophobic contacts with Met135 and the aliphatic side chain of Arg80, respectively. A detailed interaction interface is shown in Fig. 6(*b*). The model illustrates that the synthetase-domain loop adopts a conformation that is close to the N-terminal domain and by doing so is in a perfect position to induce a conformational change. The N-terminal domain is close to the glutaminase domain and after receiving an acceptor-binding signal can further transmit the signal to the glutaminase domain, thus initiating a restructuring of the glutaminase active site. This rearrangement is most likely to be facilitated by reorganization of the oxyanion-hole region, which is in close proximity to the N-terminal region, thus priming the glutaminase domain for ammonia production.

4. Conclusions

The structures of two new states depicted as state 1 and state 3 (Fig. 1b) were determined and their potential role in catalytic

coupling was investigated. There are subtle differences in the mode of ATP binding between smPurL and lgPurL, but the overall local conformation is similar in both proteins. Similarly, there is also not much difference between the glutaminase thioester-bound form and the unliganded form of StPurL. Therefore, it is most likely to be the later steps in the reaction, such as the binding of FGAR, that activate the glutaminase for catalytic coupling. This is evident because all of our soaking attempts to capture FGAR alone or FGAR with ATP in lgPurL crystals resulted in instant degradation of the StPurL crystals, hinting at a major conformational change associated with FGAR binding. In addition, modelling studies suggested that ordering of the synthetase-domain loop plays a major role in interdomain signalling. Further studies need to be pursued to capture the FGAR-bound state in order to fully comprehend the mechanism of catalytic coupling.

References

Anand, R., Hoskins, A. A., Bennett, E. M., Sintchak, M. D., Stubbe, J. & Ealick, S. E. (2004). *Biochemistry*, **43**, 10343–10352.

Anand, R., Hoskins, A. A., Stubbe, J. & Ealick, S. E. (2004). *Biochemistry*, **43**, 10328–10342.

Brünger, A. T., Adams, P. D., Clore, G. M., DeLano, W. L., Gros, P., Grosse-Kunstleve, R. W., Jiang, J.-S., Kuszewski, J., Nilges, M., Pannu, N. S., Read, R. J., Rice, L. M., Simonson, T. & Warren, G. L. (1998). *Acta Cryst.* D**54**, 905–921.

DeLano, W. L. (2002). *PyMOL*. http://www.pymol.org.

Emsley, P., Lohkamp, B., Scott, W. G. & Cowtan, K. (2010). *Acta Cryst.* D**66**, 486–501.

Fiser, A., Do, R. K. & Sali, A. (2000). *Protein Sci.* **9**, 1753–1773.

Goto, M., Omi, R., Nakagawa, N., Miyahara, I. & Hirotsu, K. (2004). *Structure*, **12**, 1413–1423.

Holden, H. M., Thoden, J. B. & Raushel, F. M. (1999). *Cell. Mol. Life Sci.* **56**, 507–522.

Hoskins, A. A., Anand, R., Ealick, S. E. & Stubbe, J. (2004). *Biochemistry*, **43**, 10314–10327.

Huang, X., Holden, H. M. & Raushel, F. M. (2001). *Annu. Rev. Biochem.* **70**, 149–180.

Jones, T. A., Zou, J.-Y., Cowan, S. W. & Kjeldgaard, M. (1991). *Acta Cryst.* A**47**, 110–119.

Kappock, T. J., Ealick, S. E. & Stubbe, J. (2000). *Curr. Opin. Chem. Biol.* **4**, 567–572.

Laskowski, R. A., MacArthur, M. W., Moss, D. S. & Thornton, J. M. (1993). *J. Appl. Cryst.* **26**, 283–291.

Leslie, A. G. W. (1997). *MOSFLM* v.5.40. MRC Laboratory of Molecular Biology, Cambridge.

Levenberg, B., Melnick, I. & Buchanan, J. M. (1957). *J. Biol. Chem.* **225**, 163–176.

Li, C., Kappock, T. J., Stubbe, J., Weaver, T. M. & Ealick, S. E. (1999). *Structure*, **7**, 1155–1166.

Li, H.-C. & Buchanan, J. M. (1971). *J. Biol. Chem.* **246**, 4720–4726.

Massière, F. & Badet-Denisot, M. A. (1998). *Cell. Mol. Life Sci.* **54**, 205–222.

McCulloch, K. M., Kinsland, C., Begley, T. P. & Ealick, S. E. (2008). *Biochemistry*, **47**, 3810–3821.

Morar, M., Anand, R., Hoskins, A. A., Stubbe, J. & Ealick, S. E. (2006). *Biochemistry*, **45**, 14880–14895.

Morar, M., Hoskins, A. A., Stubbe, J. & Ealick, S. E. (2008). *Biochemistry*, **47**, 7816–7830.

Mouilleron, S. & Golinelli-Pimpaneau, B. (2007). *Curr. Opin. Struct. Biol.* **17**, 653–664.

Myers, R. S., Amaro, R. E., Luthey-Schulten, Z. A. & Davisson, V. J. (2005). *Biochemistry*, **44**, 11974–11985.

Myers, R. S., Jensen, J. R., Deras, I. L., Smith, J. L. & Davisson, V. J. (2003). *Biochemistry*, **42**, 7013–7022.

Otwinowski, Z. & Minor, W. (1997). *Methods Enzymol.* **276**, 307–326.

Panjikar, S., Parthasarathy, V., Lamzin, V. S., Weiss, M. S. & Tucker, P. A. (2005). *Acta Cryst.* D**61**, 449–457.

Raushel, F. M., Thoden, J. B. & Holden, H. M. (1999). *Biochemistry*, **38**, 7891–7899.

Raushel, F. M., Thoden, J. B. & Holden, H. M. (2003). *Acc. Chem. Res.* **36**, 539–548.

Reissmann, S., Hochleitner, E., Wang, H., Paschos, A., Lottspeich, F., Glass, R. S. & Böck, A. (2003). *Science*, **299**, 1067–1070.

Schendel, F. J. & Stubbe, J. (1986). *Biochemistry*, **25**, 2256–2264.

Schulz, G. E. (1992). *Curr. Opin. Chem. Biol.* **2**, 61–67.

Willemoës, M., Mølgaard, A., Johansson, E. & Martinussen, J. (2005). *FEBS J.* **272**, 856–864.

Winn, M. D. *et al.* (2011). *Acta Cryst.* D**67**, 235–242.

Zhang, Y., Morar, M. & Ealick, S. E. (2008). *Cell. Mol. Life Sci.* **65**, 3699–3724.